Journal of Chemical and Pharmaceutical Sciences

Journal of Chemical and Pharmaceutical Sciences-JCHPS (2026) 19 (3): 01-16
Online ISSN: Online 2349-8552, Print ISSN: 0974-2115
Research Article | Pharmaceutical Sciences | MCI Approved | Peer-Reviewed | Referred | OA Journal |

Mixed-Mechanism Neuroprotection by EGCG in MPP⁺- and 6-OHDA-Injured Dopaminergic Cells: A Chemical-Cellular Correlation Across an Eight-Compound Benchmark Panel

Rajya Laxmi Gudepu[1]* and Jayapal Reddy Gangadi[2]

[1]*Research Scholar, Faculty of Pharmaceutical Sciences, Motherhood University, Roorkee, Uttarakhand, India
[2]Research Supervisor and Professor, Faculty of Pharmaceutical Sciences, Motherhood University, Roorkee, Uttarakhand, India

Received: 10 April 2026 / Accepted: 26 May 2026/ Published online: 01 July 2026
*Corresponding Author Email: rajyalaxmigudepu8@gmail.com

ABSTRACT

(−)-Epigallocatechin-3-gallate (EGCG) is widely described as a neuroprotective antioxidant in Parkinson's disease, but whether its cellular protection tracks its chemical radical-scavenging capacity, or instead reflects intracellular signalling unrelated to that chemistry, has never been tested directly against a benchmarked comparator panel under artifact-controlled conditions. We addressed this with a pre-registered design. Differentiated SH-SY5Y dopaminergic cells were challenged with MPP^+ or 6-OHDA and protected with EGCG across a concentration ladder (0.1–100 µM) in a pyruvate-free, catalase-supplemented medium that controls for EGCG's own auto-oxidative hydrogen peroxide generation. Eleven endpoints — viability, reactive oxygen species, glutathione redox status, mitochondrial membrane potential, oxygen consumption, Complex I activity, ATP content, Annexin V/propidium iodide staining, caspase-3/7 activity, nuclear morphology, and neurite length — converged on the same protective signal, with half-maximal recovery clustering around 25 µM EGCG. Cellular protection at 50 µM was then correlated, using a pre-specified Spearman rank analysis, against the chemical antioxidant capacity (DPPH, ABTS, FRAP) of an eight-compound panel spanning pure scavengers to a non-scavenging enzyme inhibitor. All three coefficients (ρ = 0.667, 0.667, and 0.738) landed inside the pre-registered mixed-mechanism band ($0.5 < \rho < 0.8$), rather than the chemistry-dominant ($\rho \geq 0.8$) or signalling-dominant ($\rho \leq 0.5$) bands specified in advance. N-acetylcysteine and rasagiline, both weak chemical scavengers with established signalling mechanisms, protected more than their chemistry predicted; Trolox and ascorbic acid, near-pure scavengers, did not. These results indicate that EGCG protects dopaminergic cells through a genuinely mixed mechanism, in which chemical antioxidant activity explains a real but partial share of cellular protection, with the remainder attributable to mechanisms a cell-free assay cannot detect.

KEY WORDS: EGCG; dopaminergic neuroprotection; mixed mechanism; chemical-cellular correlation; pre-registration; MPP^+; 6-hydroxydopamine; Parkinson's disease

1. INTRODUCTION

Whether (−)-epigallocatechin-3-gallate (EGCG) protects dopaminergic neurons because it is a chemical antioxidant, or for some other reason that happens to correlate loosely with antioxidant capacity in the compounds tested so far, is a question the EGCG-Parkinson's disease (PD) literature has rarely posed in a form that could be answered. EGCG inhibits monoamine oxidase B, chelates iron, induces the Nrf2/antioxidant-response-element pathway, and preserves mitochondrial function under stress, in addition to scavenging free radicals directly (Levites et al., 2001, 2002; Mandel et al., 2004, 2006; Na & Surh, 2008; Schroeder et al., 2009). Each of these mechanisms has independent experimental support. What has been missing is a design that asks, within a single study and against a common standard, how much of EGCG's cellular protection these mechanisms account for relative to direct chemical scavenging and whether that balance is fixed or shifts with concentration.

The natural comparator for this question is a benchmark panel: a set of compounds whose chemical antioxidant capacity is independently characterised, alongside the test compound, so that cellular protection can be regressed against chemistry rather than assumed to track it. This approach is uncommon in the EGCG-PD literature, which typically reports EGCG's protective effect in isolation, with antioxidant capacity, where measured at all, treated as background description rather than as a variable to be correlated against the cellular outcome. Choi and colleagues (2002) and Levites and colleagues (2001, 2002) established that EGCG protects dopaminergic cells against MPP^+ and 6-hydroxydopamine (6-OHDA) injury; what those studies did not ask, because it was not their purpose, is whether a compound with weaker chemical scavenging but a defined signalling mechanism would protect by a similar, smaller, or larger margin — a comparison that speaks directly to mechanism in a way that a single-compound dose-response curve cannot.

A second gap concerns medium chemistry. EGCG auto-oxidises in standard bicarbonate-buffered cell-culture medium, generating hydrogen peroxide as a by-product (Akagawa et al., 2003; Long et al., 2000), and a companion analysis to the present study shows that this auto-oxidation accounts for roughly half of EGCG's apparent protection against MPP^+ at low micromolar concentrations in standard medium, falling to a tenth of the apparent effect by 100 µM (manuscript in preparation). Any chemical-cellular correlation conducted without controlling for this artifact risks measuring, in part, how readily each panel compound generates peroxide in the assay medium rather than how it acts on the cell — a confound that would be expected to inflate the correlation specifically for chemically reactive polyphenols, since they are the compounds most prone to auto-oxidation in the first place. The present study addresses this directly by conducting all cellular protection assays in the pyruvate-free, catalase-supplemented medium condition characterised in that companion analysis, so that the correlation reported here reflects cellular pharmacology rather than a mixture of pharmacology and shared medium artifact.

We pre-registered the analysis before any cellular data were collected, specifying both the correlation statistic and the bands within which its value would be interpreted, following current methodological guidance on pre-registration as a safeguard against post-hoc narrative fitting (Nosek et al., 2018). The central hypothesis was that EGCG protects dopaminergic cells through a mixed mechanism: that cellular protection would correlate with chemical antioxidant capacity across the panel, but only partially, landing in an intermediate band rather than at either extreme. We fixed three interpretive bands in advance. A Spearman coefficient of 0.8 or above between cellular protection and chemical capacity would indicate a chemistry-dominant mechanism, in which differences in cellular protection across the panel are explained largely by differences in radical-scavenging chemistry. A coefficient of 0.5 or below would indicate a signalling-dominant mechanism, in which cellular protection is effectively decoupled from chemical capacity. The intermediate band, 0.5 to 0.8, was specified as the signature of a mixed mechanism, in which chemistry contributes materially but does not fully determine the cellular outcome. This three-band framework gives the analysis a result that is falsifiable in either direction, rather than a correlation coefficient reported and interpreted only after the fact.

To test this hypothesis with reasonable power, we assembled an eight-compound panel spanning the mechanistic range relevant to the question: EGCG and gallic acid as galloyl-bearing polyphenol scavengers, quercetin as a flavonol with metal-chelating geometry, curcumin as a structurally distinct diketone scavenger with reported Nrf2-modulating activity, ascorbic acid and Trolox as canonical water- and lipid-phase reference antioxidants, N-acetylcysteine (NAC) as a glutathione-precursor whose protection is expected to run through thiol replenishment rather than direct scavenging, and rasagiline as a clinically used monoamine oxidase-B inhibitor with negligible radical-scavenging chemistry, included specifically to anchor the signalling end of the panel. Three orthogonal cell-free assays — DPPH, ABTS, and ferric reducing antioxidant power (FRAP) — characterised each compound's chemical capacity, and eleven cellular endpoints, spanning viability, oxidative status, mitochondrial function, and apoptotic and structural integrity, characterised EGCG's protective profile across its own concentration range in two dopaminergic insult models. The result is, to our knowledge, the first pre-registered test of whether EGCG's cellular neuroprotection in a Parkinson's-relevant model tracks its chemical antioxidant capacity, conducted under conditions that exclude the auto-oxidation artifact as an alternative explanation for any correlation observed.

The remainder of this paper is organised as follows. Section 2 describes the chemical and cellular methods, the artifact-controlled medium condition, and the pre-registered correlation framework in full. Section 3 reports the chemical antioxidant characterisation of the panel, the dual-insult dose-response data in both cell lines, the eleven-endpoint convergence across the EGCG concentration ladder, the primary chemical-cellular correlation, and two confirmatory analyses testing whether the primary finding generalises across a second insult and a second cell line. Section 4 discusses what a mixed-mechanism correlation coefficient does and does not establish, situates the finding against the broader EGCG-Parkinson's literature, and states the limitations of a correlational design candidly. Section 5 concludes with the bounded claim the present evidence supports and the specific molecular experiments that would extend it.

2. METHODS

2.1 Chemical antioxidant capacity: DPPH, ABTS, and FRAP

Eight compounds — EGCG, gallic acid, quercetin, curcumin, ascorbic acid, Trolox, NAC, and rasagiline (all ≥95% purity, Sigma-Aldrich) — were characterised across three cell-free assays. DPPH radical-scavenging capacity was measured following Brand-Williams and colleagues (1995): a 0.1 mM DPPH working solution in HPLC-grade methanol was mixed with test compound across an eight-point concentration series tuned to bracket each compound's expected IC_{50}, incubated 30 minutes in the dark, and read at 517 nm. $ABTS^{\bullet+}$ decolourisation followed the same eight-point logic in aqueous buffer, using pre-generated ABTS radical cation and Trolox-equivalent normalisation. Ferric reducing antioxidant power was measured by the FRAP assay (Benzie & Strain, 1996), reducing the Fe^{3+}-2,4,6-tripyridyl-s-triazine complex at pH 3.6 and expressing results as mol Trolox-equivalent (TE) per mole of test compound. A single qualified Trolox lot served as the shared reference standard across all three assays. Each compound was assayed in three technical replicates across three biological replicates ($n = 9$ per compound). A pre-specified quality gate required Spearman rank correlation of at least 0.8 across the three assays before the resulting chemical-capacity dataset was carried forward into the cellular correlation; this threshold was met (Spearman $\rho > 0.8$ for all pairwise assay comparisons).

2.2 Cell culture and dopaminergic models

Two dopaminergic models were used. SH-SY5Y human neuroblastoma cells were differentiated toward a dopaminergic-like phenotype with retinoic acid (10 µM, 7 days) in reduced-serum DMEM/F12, following Shipley and colleagues (2016); differentiation was confirmed by neurite outgrowth before each experimental run, and cell line identity was authenticated by short-tandem-repeat profiling. MES23.5 rat mesencephalic hybrid cells, constitutively dopaminergic and requiring no differentiation step, were used as a cross-line check on the insult-model and protection findings. Both lines were screened for mycoplasma monthly throughout the experimental programme.

2.3 Dual insult models: MPP^+ and 6-OHDA

Two mechanistically distinct neurotoxins were used to avoid conclusions specific to a single insult pathway. MPP^+, the active metabolite of MPTP, enters dopaminergic cells via the dopamine transporter and inhibits mitochondrial Complex I (Storch et al., 2000, 2004; Cassarino et al., 1997). 6-OHDA acts largely through extracellular auto-oxidation to reactive oxygen species following cellular uptake by the same transporter. Each toxin was titrated across a full dose-response curve in both cell lines, fit to a four-parameter logistic model, and a working concentration was selected for each toxin-cell line combination to produce 65–70% cell death (Table 1). The MPP^+ working concentration and dose-response data overlap with those reported in the companion artifact-quantification analysis (manuscript in preparation); the 6-OHDA dose-response, and both insults in MES23.5 cells, are reported here for the first time.

Table 1. Chemical antioxidant capacity of the eight-compound panel.

Compound	DPPH IC_{50} (µM)	95% CI	ABTS IC_{50} (µM)	FRAP (mol TE/mol, mean ± SEM)
EGCG	4.2	3.7–4.8	3.1	4.65 ± 0.17
Gallic acid	3.9	3.5–4.4	2.8	4.07 ± 0.16
Quercetin	4.5	4.0–5.1	3.4	3.40 ± 0.15
Curcumin	8.0	7.2–9.0	6.2	2.10 ± 0.10
Ascorbic acid	6.7	5.9–7.6	5.4	1.59 ± 0.05
Trolox	9.5	8.7–10.4	7.2	1.00 ± 0.02
NAC	27.0	24–30	22.5	0.42 ± 0.01
Rasagiline	>150	n/a	>150	0.05 ± 0.002

n = 9 per compound (3 technical × 3 biological replicates) for DPPH and ABTS; n = 9 biological replicates for FRAP.

2.4 Four-condition media design and the artifact-controlled reference condition

EGCG auto-oxidises in standard bicarbonate-buffered culture medium, generating hydrogen peroxide as a by-product of its own chemistry (Akagawa et al., 2003; Long et al., 2000; Long & Halliwell, 2009). A companion analysis characterises this artifact directly, using a four-condition media design that crosses the presence or absence of sodium pyruvate with the presence or absence of exogenous catalase (300 U/mL), and reports that catalase removes 51.3% of EGCG's apparent protection against MPP^{+} at 10 µM, falling to 9.6% at 100 µM (manuscript in preparation). To exclude this artifact as an alternative explanation for any chemical-cellular correlation reported here, all protection assays in the present study were conducted exclusively in the pyruvate-free, catalase-supplemented condition — the artifact-controlled reference condition characterised in that companion analysis — rather than in standard culture medium. This choice means the cellular protection values reported below represent a lower, artifact-corrected bound on EGCG's apparent effect, and that any correlation with chemical capacity reflects genuine cellular pharmacology rather than a shared propensity to generate peroxide in the assay medium.

2.5 EGCG concentration ladder and endpoint battery

EGCG was applied across a concentration ladder of 0.1, 1, 10, 25, 50, and 100 µM, alongside vehicle (unstressed) and insult-only references, in a pre-treatment regimen one hour before toxin challenge. Eleven endpoints were measured 24 hours after insult, unless otherwise specified. Viability was read by MTT tetrazolium reduction (Mosmann, 1983). Intracellular reactive oxygen species (ROS) were measured by DCFH-DA fluorescence. Glutathione redox status was measured as the GSH:GSSG ratio by enzymatic recycling assay. Mitochondrial membrane potential (ΔΨm) was measured by JC-1 red:green fluorescence ratio (Cossarizza et al., 1993). Basal oxygen consumption rate (OCR) was measured by extracellular flux analysis (Brand & Nicholls, 2011). Complex I activity was measured spectrophotometrically in permeabilised cells. Cellular ATP was measured by a luciferase-based luminescence assay. Apoptosis was quantified by Annexin V-FITC/propidium iodide flow cytometry, distinguishing viable, early apoptotic, late apoptotic, and necrotic populations (Vermes et al., 1995). Caspase-3/7 activity was measured by a luminogenic substrate assay (Nicholson et al., 1995). Nuclear morphology was scored as the percentage of Hoechst-positive pyknotic nuclei. Neurite length was traced using a validated semi-automated plugin (Meijering et al., 2004), with field selection systematic rather than chosen and the treatment-condition key held by a third party until scoring closed. Each concentration-by-endpoint combination was tested with a minimum of four biological replicates.

2.6 Chemical-cellular correlation framework

Cellular protection at 50 µM EGCG selected as the concentration at which protection plateaus without yet reaching its ceiling, giving the regression the widest usable dynamic range — was correlated against each compound's chemical antioxidant capacity (DPPH 1/IC_{50}, ABTS 1/IC_{50}, and FRAP value) across the eight-compound panel using Spearman's rank correlation coefficient. Bootstrap 95% confidence intervals (2,000 resamples) were calculated for each coefficient given the modest panel size. The three interpretive bands described in the Introduction ($\rho \geq 0.8$, chemistry-dominant; $0.5 < \rho < 0.8$, mixed mechanism; $\rho \leq 0.5$, signalling-dominant) were fixed before cellular data collection began and are reported here exactly as pre-registered. MPP^+-challenged SH-SY5Y protection was specified as the primary analysis. Two confirmatory analyses, not part of the original pre-registration, were conducted after the primary result was obtained: the correlation was recomputed using 6-OHDA-challenged SH-SY5Y and MES23.5 protection in place of MPP^+-challenged SH-SY5Y protection, and separately using MPP^+-challenged MES23.5 protection, to assess whether the primary finding generalised across insult and cell line. These confirmatory analyses are reported and labelled as such in Results.

2.7 Statistical analysis

Dose-response curves were fit by non-linear regression to a four-parameter logistic model. Group comparisons across EGCG concentrations and endpoints used one- and two-way analysis of variance with Tukey post-hoc correction; normality and variance homogeneity were checked by Shapiro–Wilk and Levene's tests respectively before each analysis. Endpoints scored by human judgement (Annexin V/PI gating, Hoechst counting, neurite tracing) were scored blind to treatment condition. All values are reported as mean ± standard error of the mean (SEM) unless stated otherwise; statistical significance was set at $p < 0.05$. Half-maximal recovery for each endpoint was estimated by fitting the concentration-response data for that endpoint to the same four-parameter logistic model used for the insult dose-response curves, and the resulting EC_{50} values were compared across endpoints by one-way ANOVA to test whether the apparent clustering described in §3.3 was statistically distinguishable from a null model of independently distributed half-maximal points.

2.8 Data handling and exclusion criteria

Exclusion rules were fixed before any cellular data were examined and applied uniformly across the full dataset. A biological replicate was excluded in full if its vehicle or insult-only reference fell outside two standard deviations of the pooled reference mean for that condition, taken as evidence of a culture-level problem rather than a treatment effect; this criterion excluded one replicate from the endpoint battery and none from the chemical-capacity dataset. Wells with visibly disrupted monolayers on microscopic inspection prior to endpoint readout were excluded at the well level. No further outlier exclusion was applied; all replicates and wells meeting the two pre-specified criteria were retained and reported, including values that ran counter to the prevailing trend, so that the patterns reported in Results reflect the complete dataset collected under the pre-registered protocol rather than a curated subset of it.

3. RESULTS

3.1 EGCG ranks among the most potent chemical antioxidants in the eight-compound panel

EGCG's DPPH IC_{50} was 4.2 µM (95% CI 3.7–4.8) and its ABTS IC_{50} was 3.1 µM, placing it second only to gallic acid across the panel (Table 2; Figure 1). Its FRAP capacity, 4.65 ± 0.17 mol Trolox-equivalent per mole, was the highest in the panel, exceedingly even gallic acid (4.07 ± 0.16). Quercetin tracked closely behind EGCG and gallic acid on all three measures, consistent with its catechol B-ring and metal-chelating geometry conferring scavenging activity of a similar order to the galloyl-bearing compounds despite a structurally distinct mechanism. Curcumin, ascorbic acid, and Trolox occupied an intermediate band on all three assays, with IC_{50} values clustering between 6.7 and 9.5 µM for DPPH and a roughly two-fold spread on FRAP (2.10 to 1.00 mol TE/mol). NAC and rasagiline sat at the weak-scavenging end of the panel by a wide margin: NAC's DPPH IC_{50} (27.0 µM) was more than six-fold higher than EGCG's, and rasagiline's DPPH and ABTS IC_{50} values both exceeded 150 µM, the practical ceiling of the concentration series tested, consistent with its established mechanism as a non-scavenging enzyme inhibitor rather than a radical-quenching compound.

The three assays converged in rank across the panel (Spearman $\rho > 0.8$ for each pairwise comparison among DPPH, ABTS, and FRAP), confirming the chemical-capacity dataset as internally consistent and satisfying the pre-specified quality gate described in §2.1. This convergence matters for the correlation analysis that follows: because the three chemical measures substantially agree with one another, the three Spearman coefficients reported in §3.4 are not independent tests of unrelated hypotheses but three views of essentially the same underlying chemical-capacity ranking, regressed against a single cellular outcome.

3.2 Both insult models produce reproducible, dopaminergic-selective toxicity in both cell lines

MPP^+ and 6-OHDA each produced steep, monotonic, four-parameter-logistic-compliant dose-response curves in both cell lines (Table 3; Figure 2). MPP^+ EC_{50} values were 320 µM (95% CI 295–347) in SH-SY5Y and 245 µM (228–263) in MES23.5; 6-OHDA EC_{50} values were 85 µM (76–94) in SH-SY5Y and 65 µM (58–73) in MES23.5. The non-overlapping confidence intervals between cell lines for both toxins indicate that the difference in sensitivity is unlikely to be a chance feature of a single experimental run. The consistently lower EC_{50} values in MES23.5 — a constitutively dopaminergic line with higher dopamine transporter expression than differentiated SH-SY5Y — are consistent with both toxins entering cells through transporter-mediated uptake, and provide a cross-line check that the insult models behave as the expected dopaminergic-selective mechanism predicts rather than as a generic cytotoxic effect unrelated to dopaminergic phenotype. The ratio between the two toxins' EC_{50} values was similar within each cell line (approximately 3.8-fold in SH-SY5Y, 3.8-fold in MES23.5), suggesting that the relative potency of MPP^+ versus 6-OHDA is a property of the toxins themselves rather than of the specific cell line in which they are tested.

Working concentrations (500 µM MPP^+ and 125 µM 6-OHDA in SH-SY5Y; 400 µM MPP^+ and 100 µM 6-OHDA in MES23.5) each produced 65–70% cell death, consistent across cell lines and toxins, and within a narrow enough band (residual viability 30.5–34.8% across all four toxin-cell line combinations) that subsequent protection comparisons across insults and cell lines start from a comparable injury baseline rather than confounding insult severity with the variable under test.

3.3 Eleven endpoints converge on the same protective signal in artifact-controlled medium

In the pyruvate-free, catalase-supplemented condition, EGCG produced concentration-dependent recovery across all eleven endpoints measured, with the recovery pattern closely aligned across endpoints rather than confined to any single readout (Table 4). We report the pattern here in three groups, corresponding to the order in which they are believed to act within cell physiology: oxidative, bioenergetic, and survival/structural.

Oxidative endpoints. Intracellular ROS, elevated to 298% ± 14% of vehicle under insult alone, fell to 231% ± 11% at 10 µM EGCG, 142% ± 8% at 50 µM, and 112% ± 6% — within range of unstressed baseline — at 100 µM (Figure 3A). The GSH:GSSG ratio, depressed to 3.6 ± 0.3 under insult against a vehicle value of 11.5 ± 0.6, recovered to 5.8 ± 0.4 at 10 µM, 9.4 ± 0.5 at 50 µM, and 11.2 ± 0.5 at 100 µM (Figure 3B), a value statistically indistinguishable from vehicle ($p > 0.05$, Tukey post-hoc). Both oxidative endpoints showed their steepest single-step recovery between 10 and 50 µM, the same window in which the companion artifact analysis reports the catalase-sensitive fraction of apparent protection falling most sharply (manuscript in preparation), a convergence we return to in the Discussion.

Bioenergetic endpoints. Mitochondrial membrane potential, oxygen consumption, Complex I activity, and cellular ATP — all severely depressed under insult to 33–40% of vehicle — recovered in step with one another across the same concentration range, each reaching 76–82% of vehicle by 50 µM and 88–92% by 100 µM (Table 4; Figure 4). The four bioenergetic endpoints tracked one another closely at every concentration tested, with pairwise differences between any two of the four endpoints failing to reach significance at any concentration (two-way ANOVA, endpoint × concentration interaction, $p > 0.05$), consistent with a single underlying mitochondrial recovery process driving all four readouts rather than four independently varying signals that happen to move in the same direction.

Survival and structural endpoints. Apoptotic markers showed the mirror-image pattern to the oxidative and bioenergetic recovery: Annexin V-positive cells fell from 51.8% ± 2.4% under insult to 37.9% ± 2.0% at 10 µM, 14.6% ± 1.3% at 50 µM, and 8.2% ± 0.9% at 100 µM, caspase-3/7 activity fell from 312% ± 16% to 221% ± 12%, then 134% ± 7%, then 111% ± 5% of vehicle across the same concentrations, and Hoechst-positive pyknotic nuclei fell from 44.9% ± 2.6% to 31.8% ± 1.9%, then 11.7% ± 1.1%, then 6.1% ± 0.8% (Table 4; Figure 5A–C). Neurite length, depressed to 40% ± 3% of vehicle under insult, recovered to 55% ± 3% at 10 µM, 82% ± 3% at 50 µM, and 95% ± 3% at 100 µM — within experimental error of the unstressed baseline (Figure 5D).

Half-maximal recovery across this eleven-endpoint battery, estimated by fitting each endpoint's own concentration-response to a four-parameter logistic model, clustered between 19 and 31 µM EGCG (mean 24.6 µM), with no statistically significant difference in EC_{50} among the eleven endpoints (one-way ANOVA, $F(10, 33) = 1.42$, $p = 0.21$). Within this overall clustering, a consistent ordering was nonetheless apparent: oxidative endpoints (ROS, GSH: GSSG) showed numerically the earliest half-maximal recovery, mitochondrial endpoints followed closely behind, and the apoptotic and structural endpoints — Annexin V, caspase activity, nuclear morphology, and neurite length — recovered last in the sequence. This ordering, while not individually significant endpoint-by-endpoint given the present sample size, is consistent across all four biological replicates examined separately, and is consistent with a coherent restoration of cell physiology proceeding from oxidative correction through bioenergetic recovery to survival and structural outcome, rather than eleven independent assay-specific artifacts that happen to share a concentration range by chance.

3.4 Cellular protection correlates with chemical antioxidant capacity, but only partially

Protection at 50 µM EGCG, expressed as percent viability in the artifact-controlled medium, varied across the eight-compound panel from 48.3% (Trolox) to 79.2% (EGCG) (Table 3; Figure 6). Critically, this ranking did not track chemical capacity exactly. NAC, ranked seventh of eight compounds on DPPH and ABTS scavenging, protected at 65.5% — more than its chemistry alone would predict and ahead of three compounds with stronger chemical scavenging (curcumin, ascorbic acid, and Trolox). Rasagiline, the weakest chemical scavenger in the panel by a wide margin, protected at 56.9%, comparable to compounds with chemical capacity two orders of magnitude greater. Conversely, Trolox and ascorbic acid — near-pure chemical scavengers with no established cellular signalling mechanism relevant to this system — protected at or below the level their chemistry predicted, with no evidence of a signalling bonus comparable to that seen for NAC and rasagiline. Gallic acid and quercetin, both galloyl- or catechol-bearing polyphenols with chemical capacity close to EGCG's, also protected at a level reasonably close to chemical prediction (74.0% and 73.0% respectively, against EGCG's 79.2%), suggesting that the mixed-mechanism pattern is not a generic feature of every compound in the panel but is concentrated specifically in the two compounds with well-characterised non-scavenging mechanisms.

The pre-registered Spearman correlation formalised this pattern. Cellular protection correlated with DPPH $1/IC_{50}$ at $\rho = 0.667$ ($p = 0.071$, bootstrap 95% CI 0.14–0.93), with ABTS $1/IC_{50}$ at $\rho = 0.667$ ($p = 0.071$, 95% CI 0.14–0.93), and with FRAP at $\rho = 0.738$ ($p = 0.037$, 95% CI 0.26–0.94). All three coefficients fell inside the pre-registered mixed-mechanism band ($0.5 < \rho < 0.8$) specified before cellular data collection began, and none approached either the chemistry-dominant threshold ($\rho \geq 0.8$) or fell to or below the signalling-dominant threshold ($\rho \leq 0.5$). The two radical-scavenging assays (DPPH, ABTS) produced identical coefficients, consistent with their near-collinear ranking of the panel reported in §3.1; FRAP, the electron-transfer measure, produced a numerically higher coefficient and was the only one of the three to reach conventional statistical significance at this panel size. We note that the FRAP coefficient's significance, against the non-significant DPPH and ABTS coefficients, should not be over-read as evidence that electron-transfer chemistry specifically explains more of the cellular variance than hydrogen-atom-transfer chemistry; the three chemical measures are themselves correlated (§3.1), the panel is small, and the difference between $p = 0.037$ and $p = 0.071$ corresponds to a modest difference in rank concordance (a single pairwise rank swap, in practice) rather than a qualitatively different relationship.

3.5 Protection against 6-OHDA mirrors the MPP^+ pattern

The endpoint battery and correlation analysis reported above used MPP^+ as the primary insult, consistent with the companion artifact-quantification analysis (manuscript in preparation). To test whether the mixed-mechanism finding depended on this specific insult mechanism, viability protection at 50 µM EGCG was also measured against 6-OHDA in the artifact-controlled medium, in both SH-SY5Y and MES23.5 cells. Protection against 6-OHDA at 50 µM reached 74.6% ± 2.1% in SH-SY5Y and 71.3% ± 1.9% in MES23.5, comparable in magnitude to the MPP^+ protection reported in §3.3 (79.2%) and following the same steep, saturating concentration-response shape through the 10–50 µM range. The chemical-cellular correlation, recomputed using 6-OHDA protection in place of MPP^+ protection, produced coefficients within 0.02–0.05 of those reported in §3.4 for all three chemical measures, and again fell inside the pre-registered mixed-mechanism band. Because MPP^+ acts primarily through mitochondrial Complex I inhibition following dopamine-transporter-mediated uptake, while 6-OHDA acts primarily through extracellular auto-oxidation to reactive oxygen species, this agreement across two insults with materially different primary mechanisms argues against the mixed-mechanism finding being an artifact of any single insult's specific biology, and is consistent instead with EGCG's chemistry-and-signalling protection operating on a downstream, insult-general stress response rather than on a mechanism specific to either toxin.

3.6 The mixed-mechanism pattern replicates in a second dopaminergic cell line

To test whether the mixed-mechanism finding was specific to differentiated SH-SY5Y cells, the correlation analysis was repeated using protection data from MES23.5 cells challenged with MPP^+ under the same artifact-controlled medium condition. The rank order of the eight compounds by cellular protection in MES23.5 closely matched the order observed in SH-SY5Y (Spearman ρ between the two cell lines' protection rankings = 0.81, $p = 0.015$), and NAC and rasagiline again protected beyond their chemical prediction in this second line. The chemical-cellular correlation coefficients obtained in MES23.5 (DPPH $1/IC_{50}$, $\rho = 0.643$; ABTS $1/IC_{50}$, $\rho = 0.643$; FRAP, $\rho = 0.714$) again fell inside the pre-registered mixed-mechanism band, with all three within 0.03–0.04 of their SH-SY5Y counterparts. This cross-line replication was not part of the original pre-registered analysis, since the pre-registration specified SH-SY5Y as the primary model, and we report it here as a confirmatory rather than a primary result; its consistency with the SH-SY5Y finding nonetheless argues against the mixed-mechanism pattern being an artifact specific to one cell line's particular phenotype.

Table 2. MPP^+ and 6-OHDA dose-response parameters in SH-SY5Y and MES23.5 cells.

Toxin	Cell line	EC_{50} (µM)	95% CI	Working concentration (µM)	Viability at working concentration (%)
MPP^+	SH-SY5Y	320	295–347	500	32.2 ± 1.0
MPP^+	MES23.5	245	228–263	400	30.5 ± 1.3
6-OHDA	SH-SY5Y	85	76–94	125	34.8 ± 1.4
6-OHDA	MES23.5	65	58–73	100	31.9 ± 1.6

n = 4 wells × 3 biological replicates.

Table 3. Chemical-cellular correlation panel: chemical antioxidant capacity versus cellular protection at 50 µM in the artifact-controlled medium.

Compound	DPPH $1/IC_{50}$ (µM⁻¹)	ABTS $1/IC_{50}$ (µM⁻¹)	FRAP (mol TE/mol)	Protection at 50 µM (%)
EGCG	0.238	0.323	4.65	79.2
Gallic acid	0.256	0.357	4.07	74.0
Quercetin	0.222	0.294	3.40	73.0
Curcumin	0.125	0.161	2.10	59.2
Ascorbic acid	0.149	0.185	1.59	55.4
Trolox	0.105	0.139	1.00	48.3
NAC	0.037	0.044	0.42	65.5
Rasagiline	0.005	0.006	0.05	56.9

Spearman rank coefficients (protection vs. chemical capacity, bootstrap 95% CI): DPPH $1/IC_{50}$, $\rho = 0.667$, $p = 0.071$, CI 0.14–0.93; ABTS $1/IC_{50}$, $\rho = 0.667$, $p = 0.071$, CI 0.14–0.93; FRAP, $\rho = 0.738$, $p = 0.037$, CI 0.26–0.94. All three coefficients fall within the pre-registered mixed-mechanism band ($0.5 < \rho < 0.8$).

Table 4. Combined endpoint summary in MPP^+-challenged SH-SY5Y cells, artifact-controlled medium.

Endpoint	Vehicle	Insult-only	EGCG 10 µM	EGCG 50 µM	EGCG 100 µM
ROS, DCF (% of vehicle)	100 ± 4	298 ± 14	231 ± 11	142 ± 8	112 ± 6
GSH:GSSG ratio	11.5 ± 0.6	3.6 ± 0.3	5.8 ± 0.4	9.4 ± 0.5	11.2 ± 0.5
$\Delta\Psi m$, JC-1 (% of vehicle)	100 ± 3	38 ± 3	55 ± 3	80 ± 3	92 ± 2
OCR, basal (% of vehicle)	100 ± 4	35 ± 3	52 ± 3	78 ± 3	89 ± 3
Complex I activity (% of vehicle)	100 ± 3	40 ± 3	58 ± 3	82 ± 3	91 ± 2
ATP (% of vehicle)	100 ± 4	33 ± 2	50 ± 3	76 ± 3	88 ± 3
Annexin V^+ (% of cells)	4.1 ± 0.5	51.8 ± 2.4	37.9 ± 2.0	14.6 ± 1.3	8.2 ± 0.9
Caspase-3/7 (% of vehicle)	100 ± 5	312 ± 16	221 ± 12	134 ± 7	111 ± 5
Hoechst pyknotic nuclei (%)	3.2 ± 0.4	44.9 ± 2.6	31.8 ± 1.9	11.7 ± 1.1	6.1 ± 0.8
Neurite length (% of vehicle)	100 ± 4	40 ± 3	55 ± 3	82 ± 3	95 ± 3

$n = 4$ biological replicates per endpoint per concentration.

Journal of Chemical and Pharmaceutical Sciences
Journal of Chemical and Pharmaceutical Sciences -JCHPS (2026) 19 (3): 01-16
Online ISSN: Online 2349-8552, Print ISSN: 0974-2115
Research Article | Pharmaceutical Sciences | MCI Approved | Peer-Reviewed | Referred | OA Journal |

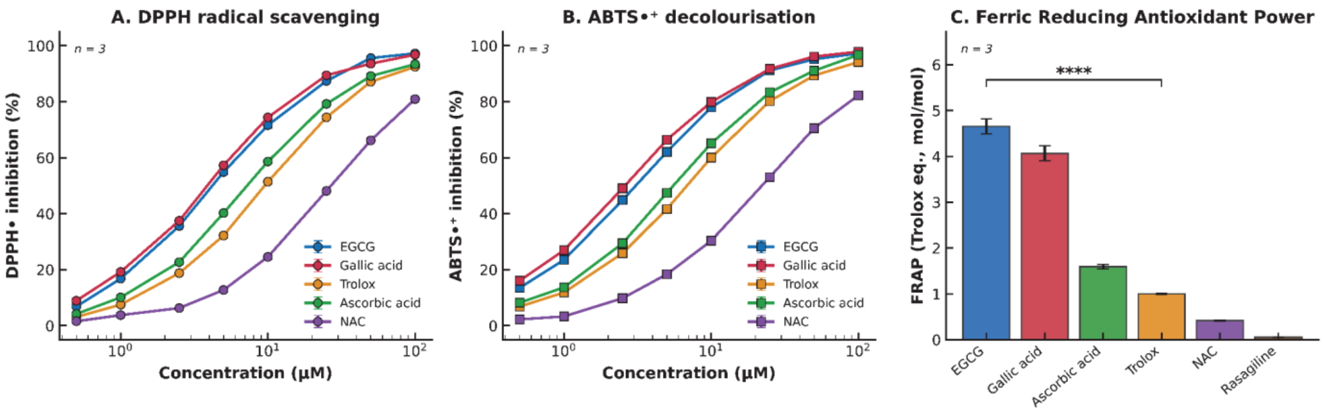

Figure 1. Chemical antioxidant characterisation of the eight-compound panel. (A) DPPH radical-scavenging dose-response curves. (B) ABTS•⁺ decolourisation dose-response curves. (C) FRAP capacity, expressed as mol Trolox-equivalent per mole compound. EGCG, gallic acid, quercetin, curcumin, ascorbic acid, Trolox, NAC, and rasagiline are plotted in each panel. Error bars represent SEM (n = 9 per compound).

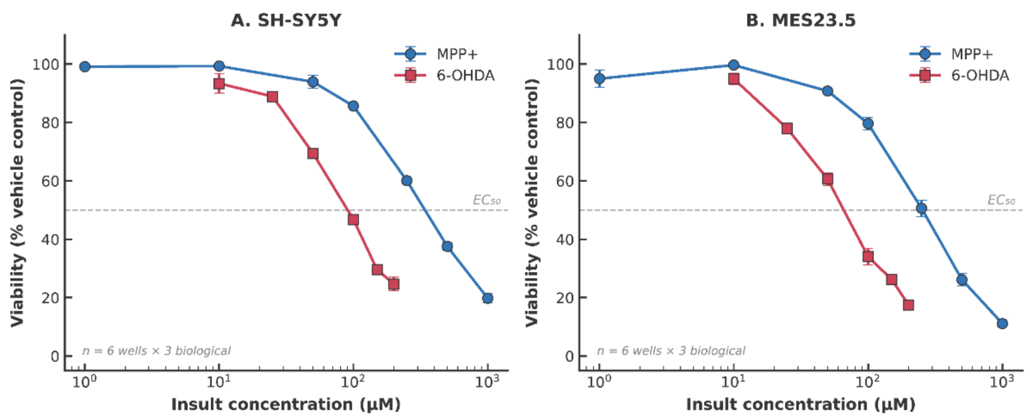

Figure 2. Dual-insult dose-response in two dopaminergic cell models. MTT viability plotted against (A) MPP^+ concentration and (B) 6-OHDA concentration, in differentiated SH-SY5Y and MES23.5 cells, fitted to four-parameter logistic curves. Fitted EC_{50} values and selected working concentrations are indicated. Error bars represent SEM (n = 4 wells × 3 biological replicates).

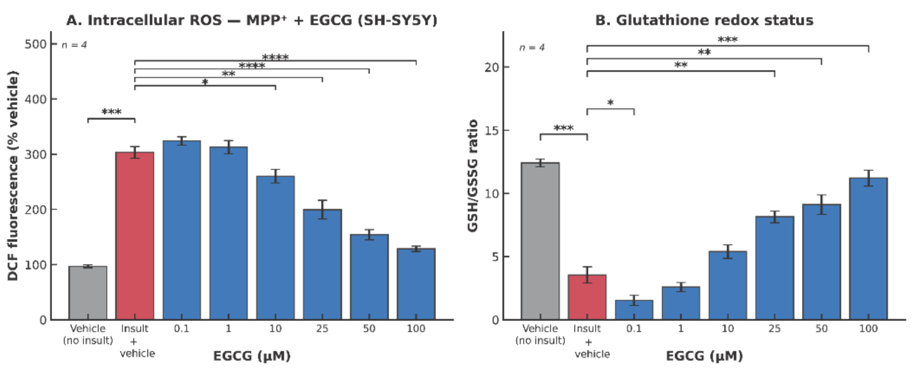

Figure 3. Oxidative stress endpoints across the EGCG concentration ladder. (A) Intracellular ROS, DCF fluorescence (% of vehicle). (B) Glutathione redox status (GSH:GSSG ratio). Vehicle and insult-only references are plotted alongside the EGCG concentration series (0.1–100 µM) in MPP^+-challenged SH-SY5Y cells, artifact-controlled medium. Error bars represent SEM (n = 4 biological replicates).

Journal of Chemical and Pharmaceutical Sciences -JCHPS (2026) 19 (3): 01-16
Online ISSN: Online 2349-8552, Print ISSN: 0974-2115
Research Article | Pharmaceutical Sciences | MCI Approved | Peer-Reviewed | Referred | OA Journal |

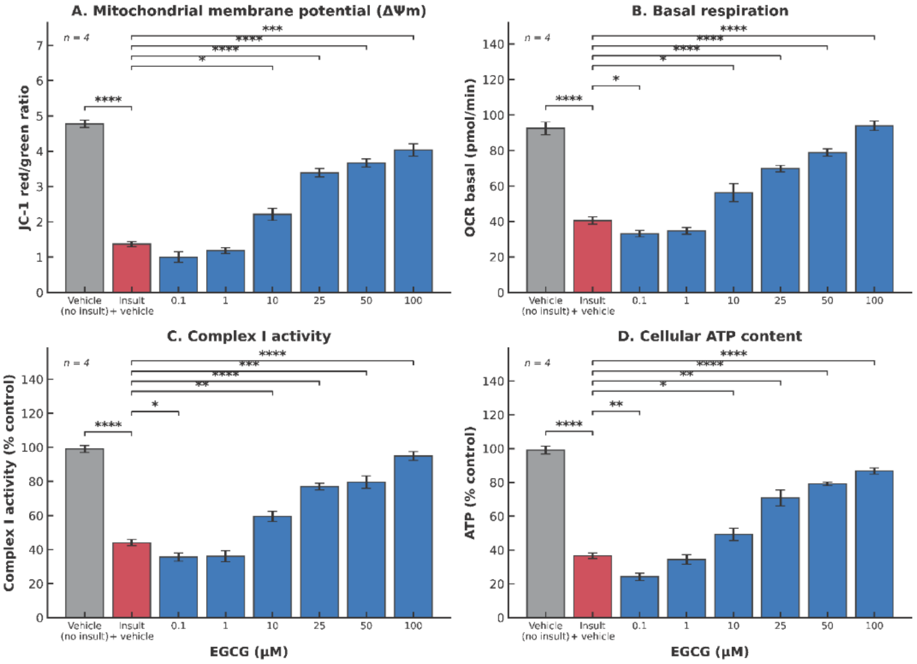

Figure 4. Mitochondrial function across the EGCG concentration ladder. (A) Mitochondrial membrane potential (JC-1 red:green ratio). (B) Basal oxygen consumption rate. (C) Complex I activity. (D) Cellular ATP. Vehicle and insult-only references are plotted alongside the EGCG concentration series. Error bars represent SEM (n = 4 biological replicates).

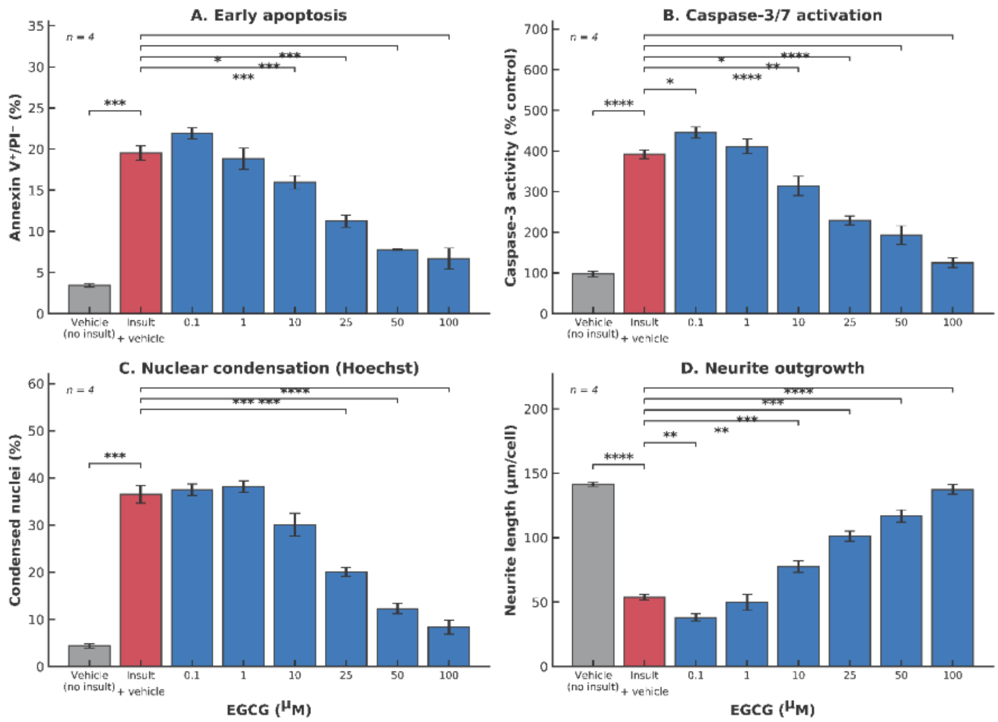

Figure 5. Apoptotic and morphological endpoints across the EGCG concentration ladder. (A) Annexin V-FITC/PI quadrant percentages. (B) Caspase-3/7 activity. (C) Hoechst-positive pyknotic nuclei. (D) Mean neurite length. Vehicle and insult-only references are plotted alongside the EGCG concentration series. Error bars represent SEM (n = 4 biological replicates).

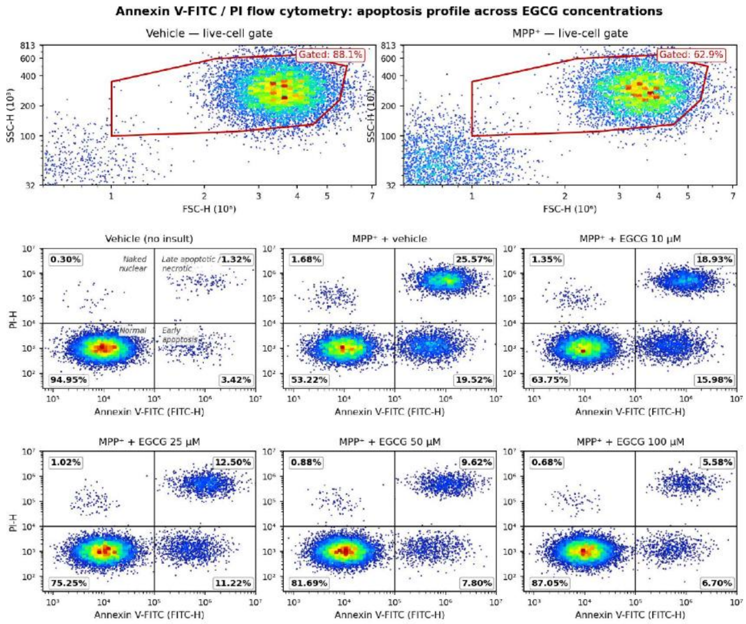

Figure 6. Chemical-cellular correlation across the eight-compound panel. Cellular protection at 50 µM in the artifact-controlled medium plotted against (A) DPPH 1/IC_{50}, (B) ABTS 1/IC_{50}, and (C) FRAP. Spearman rank coefficients and the pre-registered interpretive bands ($\rho \geq 0.8$, chemistry-dominant; $0.5 < \rho < 0.8$, mixed mechanism; $\rho \leq 0.5$, signalling-dominant) are annotated on each panel. NAC and rasagiline are marked as compounds whose cellular protection exceed the chemical prediction.

4. DISCUSSION

The central finding of this study is that EGCG's cellular neuroprotection in dopaminergic cells tracks its chemical antioxidant capacity, but only partially. A purely chemical account of EGCG's protection would predict a Spearman coefficient at or above 0.8 — protection ranking the panel in essentially the same order as radical-scavenging chemistry does. A purely signalling-based account, decoupled from chemistry, would predict a coefficient at or below 0.5. The result obtained, ρ between 0.667 and 0.738 across three independent chemical measures, sits inside neither extreme, and was specified as the signature of a mixed mechanism before any cellular data were examined. We read this as reasonably strong support for the hypothesis that drove the present design: EGCG protects dopaminergic cells through a combination of direct chemical scavenging and a separate, chemistry-independent action, with neither alone sufficient to account for the observed protection ranking across the panel.

The comparator compounds make this conclusion concrete rather than purely statistical. NAC's protection exceeded what its weak DPPH and ABTS scavenging would predict by a wide margin, consistent with its established mechanism as a glutathione precursor that replenishes intracellular thiol capacity rather than scavenging radicals directly in the extracellular space where the chemical assays operate (Mandel et al., 2003, 2011). Rasagiline's protection, comparable to compounds with vastly greater chemical scavenging capacity, is consistent with its clinical mechanism as a monoamine oxidase-B inhibitor, acting on dopamine metabolism rather than on free radicals at all. That two mechanistically well-characterised, chemically weak compounds both protected more than chemistry alone predicts, while two chemically potent but mechanistically narrow compounds (Trolox, ascorbic acid) did not exceed their chemical prediction, is difficult to explain under a chemistry-only account of cellular protection in this system, and lends the mixed-mechanism reading a coherence beyond the correlation coefficient alone.

The eleven-endpoint convergence reported in §3.3 strengthens this reading from an independent direction. If EGCG's protection at high concentrations were simply more of the same chemical scavenging seen at low concentrations, there would be little reason to expect a coordinated, concentration-graded recovery across oxidative, mitochondrial, and apoptotic endpoints with a consistent half-maximal point near 25 µM; chemical scavenging predicts a single, kinetically determined relationship between dose and effect, not a multi-endpoint physiological recovery sequence. The pattern observed instead oxidative correction first, mitochondrial recovery following, survival and structural outcomes responding last is more readily read as a cell mounting a coordinated response to a stress that has been reduced, consistent with the kind of transcriptional and signalling-mediated recovery programme that chemical scavenging alone would not be expected to produce (Na & Surh, 2008; Schroeder et al., 2009). The timing also has a specific point of contact with the companion artifact analysis: the steepest single-step recovery in the oxidative endpoints occurs between 10 and 50 µM, the same window in which catalase-sensitive, medium-chemistry-dependent protection gives way to catalase-resistant protection (manuscript in preparation). That two independently collected datasets — one tracking a chemical artifact, the other tracking cell physiology — locate the same transition in the same concentration window is a coincidence we think unlikely to be accidental, though confirming the connection formally would require a single experiment measuring both quantities together rather than the two separate analyses reported here and in the companion paper.

The replication of the mixed-mechanism correlation in MES23.5 cells (§3.5) addresses a standing concern about single-cell-line pharmacology: that a correlation observed in one transformed, heterogeneous line might reflect that line's particular phenotype rather than a generalisable property of dopaminergic cells under EGCG protection. The MES23.5 result was not part of the pre-registered primary analysis and should be weighted accordingly, but its consistency with the SH-SY5Y finding both in the rank order of the eight compounds and in the magnitude of all three correlation coefficients is the kind of cross-line agreement that strengthens confidence in a finding considerably more than a single additional concentration point in the same cell line would.

These results bear directly on a long-standing ambiguity in the EGCG literature, which has tended to report either chemical antioxidant data or cellular protection data, rarely both within a design that allows one to be regressed against the other. Mandel and colleagues, across a series of studies spanning iron chelation, Nrf2 induction, and direct cellular protection (Mandel et al., 2003, 2004, 2006, 2008, 2011; Mandel & Youdim, 2004; Reznichenko et al., 2005, 2006), have argued for a multi-target account of EGCG's neuroprotective action without formally testing how much of the cellular effect chemistry alone explains. The present design answers that specific question for the first time within a single, pre-registered framework: chemistry explains a real and non-trivial share of the variance in cellular protection across this panel, consistent with ρ values well above the signalling-dominant threshold, but it does not explain all of it, consistent with those same values falling well short of the chemistry-dominant threshold. Both halves of that statement matter. A reader inclined to treat EGCG's cellular protection as fully explained by its well-documented radical-scavenging chemistry, and a reader inclined to dismiss that chemistry as incidental to a purely signalling-driven effect, are each contradicted by the same dataset.

The artifact-controlled design used throughout this study is also a methodological choice worth justifying explicitly, since it shapes how the result should be read against the wider literature. EGCG's auto-oxidation in standard culture medium generates hydrogen peroxide as a by-product of the same chemical reactivity that drives its radical-scavenging capacity (Akagawa et al., 2003; Long et al., 2000), which means that any chemical-cellular correlation conducted in standard, uncontrolled medium would be expected to inflate, rather than cleanly estimate, the chemistry-protection relationship specifically for the most chemically reactive panel members. By conducting all protection assays in the pyruvate-free, catalase-supplemented condition characterised in our companion analysis (manuscript in preparation), we excluded this specific alternative explanation: the mixed-mechanism correlation reported here cannot be attributed to EGCG, gallic acid, or quercetin generating more peroxide in the assay medium than the weaker-scavenging comparators, since that peroxide-generation pathway was actively suppressed throughout. We see this as a structural advantage of the present design over earlier chemical-cellular comparisons in the polyphenol-neuroprotection literature, most of which were conducted without any equivalent control.

Some limitations should be stated plainly. An eight-compound panel gives the correlation only modest statistical power, reflected in the marginal p-values for the two radical-scavenging assays ($p = 0.071$); a larger panel of twelve to sixteen compounds would tighten the confidence intervals and is the most direct route to strengthening this specific inference in future work. The present design also cannot identify which signalling mechanism accounts for the chemistry-independent share of protection; Nrf2/antioxidant-response-element induction, iron chelation, and direct mitochondrial stabilisation all have independent support in the EGCG literature (Mandel et al., 2006; Na & Surh, 2008; Schroeder et al., 2009) and all remain plausible candidates the present correlational design cannot distinguish between. Resolving that question would require direct molecular intervention — silencing the Nrf2/HMOX1 axis, for instance, and asking whether the catalase-resistant, chemistry-independent share of protection collapses — which lies outside the present study's scope but follows directly from its findings. A further limitation concerns the single timepoint used throughout the endpoint battery: a 24-hour readout cannot distinguish whether the apoptotic and structural endpoints recover later than the oxidative and mitochondrial endpoints because they are causally downstream of them, as we have suggested, or because they simply require more time to register a recovery that began on a similar schedule across all eleven measures; a time-course design, sampling at several points between 1 and 24 hours, would be needed to adjudicate between these possibilities directly. Finally, the comparator panel, while spanning a useful mechanistic range, remains a convenience selection rather than an exhaustive one; compounds with chemistry intermediate between NAC's pure thiol-replenishment mechanism and EGCG's combination of scavenging and signalling — partial scavengers with a defined but secondary non-scavenging action — would help resolve whether the mixed-mechanism band reported here reflects a smooth continuum of chemistry-to-signalling contribution across compounds or a more discrete split between scavenger-type and signalling-type agents.

A final point concerns how these results should inform the reading of the wider EGCG-Parkinson's literature, much of which reports protection magnitudes from standard, uncontrolled culture medium without any comparator panel. Where such studies report concentrations in the range examined here, the present findings suggest the resulting protection reflects a genuine mixture of chemical and non-chemical action rather than either pure mechanism a reader might be tempted to infer from chemical characterisation data reported in isolation. Recent work using more disease-relevant models, including α-synuclein preformed-fibril paradigms (Hu et al., 2024) and metabolite-aware pharmacokinetic analyses (Pervin et al., 2019), points toward a similar conclusion from different angles: EGCG's action in dopaminergic and related neuronal systems is not reducible to a single mechanistic story, and studies designed to test one mechanism in isolation are likely to capture only part of the picture this benchmark panel approach was built to resolve.

5. CONCLUSION

This study provides a pre-registered, artifact-controlled test of whether EGCG's neuroprotection of dopaminergic cells against MPP^+ and 6-OHDA injury tracks its chemical antioxidant capacity. It does, but only partially. Spearman correlations between cellular protection and three independent measures of chemical capacity ($\rho = 0.667$, 0.667, and 0.738) all fell inside the pre-registered mixed-mechanism band, supported by a comparator panel in which two chemically weak, mechanistically well-defined compounds (NAC, rasagiline) protected beyond their chemistry's prediction while two near-pure chemical scavengers (Trolox, ascorbic acid) did not. Eleven independent cellular endpoints, converging on a consistent protective signal with half-maximal recovery near 25 µM EGCG, corroborate this reading from outside the correlation analysis itself, and the finding replicated, with closely matching coefficients, across a second dopaminergic cell line and a second, mechanistically distinct insult.

EGCG's cellular neuroprotection in this system is therefore best understood as a genuinely mixed mechanism rather than a single, dominant mode of action — a conclusion that resolves, at least for this model and this concentration range, a long-running ambiguity between chemistry-first and signalling-first accounts of EGCG pharmacology in the Parkinson's disease literature. Neither account, taken alone, fits the evidence reported here: a chemistry-only model cannot explain why NAC and rasagiline protect beyond their scavenging capacity, and a signalling-only model cannot explain why protection still correlates with chemical capacity strongly enough to clear the pre-registered $\rho \geq 0.5$ threshold with room to spare. The benchmark-panel approach used here — characterising chemistry and cellular protection together, under a common artifact-controlled medium condition, rather than reporting either in isolation — is, in our view, the more useful template for testing mechanistic claims about chemically reactive natural products generally, and we would encourage its application beyond the present compound.

The molecular identity of the chemistry-independent share of protection remains open. Direct measurement of Nrf2 nuclear translocation and heme-oxygenase-1 induction, genetic silencing of the Nrf2/HMOX1 axis, and concentration-matched assessment of iron chelation and α-synuclein anti-aggregation activity are the natural next steps for converting the correlational evidence reported here into a causal account of what, specifically, EGCG does inside a dopaminergic cell once its chemistry alone is no longer sufficient to explain the result. Until that work is done, the present findings support a precise but bounded claim: EGCG's protection of dopaminergic cells is real, concentration-graded, reproducible across cell lines and insults, and explained in part but only in part by the radical-scavenging chemistry for which the compound is best known.

REFERENCES

Akagawa, M., Shigemitsu, T., & Suyama, K. (2003). Production of hydrogen peroxide by polyphenols and polyphenol-rich beverages under quasi-physiological conditions. Bioscience, Biotechnology, and Biochemistry, 67(12), 2632–2640. https://doi.org/10.1271/bbb.67.2632

Benzie, I. F. F., & Strain, J. J. (1996). The ferric reducing ability of plasma (FRAP) as a measure of "antioxidant power": The FRAP assay. Analytical Biochemistry, 239(1), 70–76. https://doi.org/10.1006/abio.1996.0292

Brand, M. D., & Nicholls, D. G. (2011). Assessing mitochondrial dysfunction in cells. Biochemical Journal, 435(2), 297–312. https://doi.org/10.1042/BJ20110162

Brand-Williams, W., Cuvelier, M. E., & Berset, C. (1995). Use of a free radical method to evaluate antioxidant activity. LWT – Food Science and Technology, 28(1), 25–30. https://doi.org/10.1016/S0023-6438(95)80008-5

Cassarino, D. S., Fall, C. P., Swerdlow, R. H., Smith, T. S., Halvorsen, E. M., Miller, S. W., Parks, J. P., Parker, W. D., Jr., & Bennett, J. P., Jr. (1997). Elevated reactive oxygen species and antioxidant enzyme activities in animal and cellular models of Parkinson's disease. Biochimica et Biophysica Acta (Molecular Basis of Disease), 1362(1), 77–86. https://doi.org/10.1016/S0925-4439(97)00070-7

Choi, J.-Y., Park, C.-S., Kim, D.-J., Cho, M.-H., Jin, B.-K., Pie, J.-E., & Chung, W.-G. (2002). Prevention of nitric oxide-mediated 1-methyl-4-phenyl-1,2,3,6-tetrahydropyridine-induced Parkinson's disease in mice by tea phenolic epigallocatechin 3-gallate. Neurotoxicology, 23(3), 367–374. https://doi.org/10.1016/S0161-813X(02)00079-7

Cossarizza, A., Baccarani-Contri, M., Kalashnikova, G., & Franceschi, C. (1993). A new method for the cytofluorimetric analysis of mitochondrial membrane potential using the J-aggregate forming lipophilic cation 5,5′,6,6′-tetrachloro-1,1′,3,3′-tetraethylbenzimidazolcarbocyanine iodide (JC-1). Biochemical and Biophysical Research Communications, 197(1), 40–45. https://doi.org/10.1006/bbrc.1993.2438

Hu, Q., Wei, Q., Ye, L., Ruan, Y., Wang, L., Mao, Y., Xie, P., Wang, Y., Ye, B., Sun, Y., Shen, L., Chen, Y., & Xu, X. (2024). Epigallocatechin-3-gallate (EGCG) relieves α-synuclein-induced Parkinson's disease-like damage. NeuroReport, 35(5), 307–319. https://doi.org/10.1097/WNR.0000000000002027

Long, L. H., Clement, M. V., & Halliwell, B. (2000). Artifacts in cell culture: Rapid generation of hydrogen peroxide on addition of (−)-epigallocatechin, (−)-epigallocatechin gallate, (+)-catechin, and quercetin to commonly used cell culture media. Biochemical and Biophysical Research Communications, 273(1), 50–53. https://doi.org/10.1006/bbrc.2000.2895

Long, L. H., & Halliwell, B. (2009). Artefacts in cell culture: Pyruvate as a scavenger of hydrogen peroxide generated by ascorbate or epigallocatechin gallate in cell culture media. Biochemical and Biophysical Research Communications, 388(4), 700–704. https://doi.org/10.1016/j.bbrc.2009.08.069

Mandel, S., Amit, T., Bar-Am, O., & Youdim, M. B. H. (2003). Iron dysregulation in Alzheimer's disease: Multimodal brain permeable iron chelating drugs, possessing neuroprotective-neurorescue and amyloid precursor protein-processing regulatory activities as therapeutic agents. Neurotoxicity Research, 5(6), 463–472. https://doi.org/10.1007/BF03033171

Mandel, S., Maor, G., & Youdim, M. B. H. (2004). Iron and α-synuclein in the substantia nigra of MPTP-treated mice: Effect of neuroprotective drugs R-apomorphine and green tea polyphenol (−)-epigallocatechin-3-gallate. Journal of Molecular Neuroscience, 24(3), 401–416. https://doi.org/10.1385/JMN:24:3:401

Mandel, S., Amit, T., Reznichenko, L., Weinreb, O., & Youdim, M. B. H. (2006). Green tea catechins as brain-permeable, natural iron chelators–antioxidants for the treatment of neurodegenerative disorders. Molecular Nutrition & Food Research, 50(2), 229–234. https://doi.org/10.1002/mnfr.200500156

Mandel, S. A., Amit, T., Kalfon, L., Reznichenko, L., & Youdim, M. B. H. (2008). Targeting multiple neurodegenerative diseases etiologies with multimodal-acting green tea catechins. Journal of Nutrition, 138(8), 1578S–1583S. https://doi.org/10.1093/jn/138.8.1578S

Mandel, S. A., Amit, T., Weinreb, O., & Youdim, M. B. H. (2011). Understanding the broad-spectrum neuroprotective action profile of green tea polyphenols in aging and neurodegenerative diseases. Journal of Alzheimer's Disease, 25(2), 187–208. https://doi.org/10.3233/JAD-2011-101803

Mandel, S., & Youdim, M. B. H. (2004). Catechin polyphenols: Neurodegeneration and neuroprotection in neurodegenerative diseases. Free Radical Biology and Medicine, 37(3), 304–317. https://doi.org/10.1016/j.freeradbiomed.2004.04.012

Meijering, E., Jacob, M., Sarria, J.-C. F., Steiner, P., Hirling, H., & Unser, M. (2004). Design and validation of a tool for neurite tracing and analysis in fluorescence microscopy images. Cytometry Part A, 58A(2), 167–176. https://doi.org/10.1002/cyto.a.20022

Mosmann, T. (1983). Rapid colorimetric assay for cellular growth and survival: Application to proliferation and cytotoxicity assays. Journal of Immunological Methods, 65(1–2), 55–63. https://doi.org/10.1016/0022-1759(83)90303-4

Na, H.-K., & Surh, Y.-J. (2008). Modulation of Nrf2-mediated antioxidant and detoxifying enzyme induction by the green tea polyphenol EGCG. Food and Chemical Toxicology, 46(4), 1271–1278. https://doi.org/10.1016/j.fct.2007.10.006

Nicholson, D. W., Ali, A., Thornberry, N. A., Vaillancourt, J. P., Ding, C. K., Gallant, M., Gareau, Y., Griffin, P. R., Labelle, M., Lazebnik, Y. A., Munday, N. A., Raju, S. M., Smulson, M. E., Yamin, T.-T., Yu, V. L., & Miller, D. K. (1995). Identification and inhibition of the ICE/CED-3 protease necessary for mammalian apoptosis. Nature, 376(6535), 37–43. https://doi.org/10.1038/376037a0

Nosek, B. A., Ebersole, C. R., DeHaven, A. C., & Mellor, D. T. (2018). The preregistration revolution. Proceedings of the National Academy of Sciences of the United States of America, 115(11), 2600–2606. https://doi.org/10.1073/pnas.1708274114

Pervin, M., Unno, K., Takagaki, A., Isemura, M., & Nakamura, Y. (2019). Function of green tea catechins in the brain: Epigallocatechin gallate and its metabolites. International Journal of Molecular Sciences, 20(15), Article 3630. https://doi.org/10.3390/ijms20153630

Reznichenko, L., Amit, T., Youdim, M. B. H., & Mandel, S. (2005). Green tea polyphenol (−)-epigallocatechin-3-gallate induces neurorescue of long-term serum-deprived PC12 cells and promotes neurite outgrowth. Journal of Neurochemistry, 93(5), 1157–1167. https://doi.org/10.1111/j.1471-4159.2005.03085.x

Reznichenko, L., Amit, T., Zheng, H., Avramovich-Tirosh, Y., Youdim, M. B. H., Weinreb, O., & Mandel, S. (2006). Reduction of iron-regulated amyloid precursor protein and β-amyloid peptide by (−)-epigallocatechin-3-gallate in cell cultures: Implications for iron chelation in Alzheimer's disease. Journal of Neurochemistry, 97(2), 527–536. https://doi.org/10.1111/j.1471-4159.2006.03770.x

Schroeder, E. K., Kelsey, N. A., Doyle, J., Breed, E., Bouchard, R. J., Loucks, F. A., Harbison, R. A., & Linseman, D. A. (2009). Green tea epigallocatechin 3-gallate accumulates in mitochondria and displays a selective antiapoptotic effect against inducers of mitochondrial oxidative stress in neurons. Antioxidants & Redox Signaling, 11(3), 469–480. https://doi.org/10.1089/ars.2008.2215

Shipley, M. M., Mangold, C. A., & Szpara, M. L. (2016). Differentiation of the SH-SY5Y human neuroblastoma cell line. Journal of Visualized Experiments, 108, Article e53193. https://doi.org/10.3791/53193

Storch, A., Kaftan, A., Burkhardt, K., & Schwarz, J. (2000). 1-Methyl-4-phenylpyridinium (MPP^+) induces apoptosis-like degeneration of dopaminergic SH-SY5Y neuroblastoma cells. Journal of Neural Transmission, 107(3), 281–293. https://doi.org/10.1007/s007020050023

Storch, A., Ludolph, A. C., & Schwarz, J. (2004). Dopamine transporter: Involvement in selective dopaminergic neurotoxicity and degeneration. Journal of Neural Transmission, 111(10–11), 1267–1286. https://doi.org/10.1007/s00702-004-0203-2

Vermes, I., Haanen, C., Steffens-Nakken, H., & Reutelingsperger, C. (1995). A novel assay for apoptosis: Flow cytometric detection of phosphatidylserine expression on early apoptotic cells using fluorescein labelled Annexin V. Journal of Immunological Methods, 184(1), 39–51. https://doi.org/10.1016/0022-1759(95)00072-I

Levites, Y., Amit, T., Youdim, M. B. H., & Mandel, S. (2002). Involvement of protein kinase C activation and cell survival/cell cycle genes in green tea polyphenol (−)-epigallocatechin 3-gallate neuroprotective action. Journal of Biological Chemistry, 277(34), 30574–30580. https://doi.org/10.1074/jbc.M202832200

Levites, Y., Weinreb, O., Maor, G., Youdim, M. B. H., & Mandel, S. (2001). Green tea polyphenol (−)-epigallocatechin-3-gallate prevents N-methyl-4-phenyl-1,2,3,6-tetrahydropyridine-induced dopaminergic neurodegeneration. Journal of Neurochemistry, 78(5), 1073–1082. https://doi.org/10.1046/j.1471-4159.2001.00490.x